Microporous and Mesoporous Materials 396 (2025) 113704

Contents lists available at ScienceDirect

Microporous and Mesoporous Materials

journal homepage: www.elsevier.com/locate/micromeso

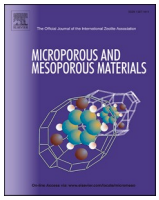

Potential of pumice scraps compared to zeolitized tuff for Mn^{2+} release in agricultural applications

Giulio Galamini [a,*], Altimari Fabiana [b], Barbieri Luisa [b,c], Malavasi Gianluca [a], Malferrari Daniele [a,c]

[a] Department of Chemical and Geological Sciences – University of Modena and Reggio Emilia, Via G. Campi 103, 41125, Modena, Italy
[b] Department of Engineering "Enzo Ferrari" – University of Modena and Reggio Emilia, Via P. Vivarelli 10, 41125, Modena, Italy
[c] BIOGEST-SITEIA, Piazzale Europa 1a, 42124, Reggio Emilia, Italy

ARTICLE INFO

Keywords:
Pumice scraps
Zeolites
Quarry waste
Manganese fertilizer
Sustainability
Recycling

ABSTRACT

Quarry waste and by-products pose significant environmental and economic challenges for the mining industry. This study investigates the potential of pumice scraps as carriers for Mn^{2+} to crops for foliar fertilization. Kinetic and Isotherm modelling were performed for Mn^{2+}-enrichment and release, and Mn^{2+} saturation level was compared to theoretical cation exchange capacity (CEC). Synthetic groundwater was used to simulate agricultural conditions in spraying machines. Pumice scraps were compared with more commonly studied zeolitized tuff (chabazite-rich). Despite its higher amorphous content (87.5 wt%) and lower zeolitic mineral content (analcime, 0.80 wt%), pumice exhibited greater affinity for Mn^{2+}, achieving higher saturation percentage of the theoretical CEC than the zeolitized tuff. Pumice also demonstrated a more stable enrichment and release, making it a promising material for delivering Mn^{2+} to crops. The use of pumice scraps in foliar fertilization could therefore represent a new way to valorise quarry waste materials.

1. Introduction

Water, soil, and air are essential resources for human life quality. However, their excessive exploitation often leads to environmental degradation. To mitigate anthropogenic impacts, many countries are adopting strategic plans for conservation, best practices in resource utilization, prevention of resource degradation, and initiatives for reusing and recycling waste materials. For instance, the Agenda 2030 for Sustainable Development is a comprehensive action program aimed at achieving specific environmental, economic, social, and institutional objectives by 2030 [1]. Consequently, the sustainable use of resources – which limits the use of virgin materials in favour of waste – is universally perceived as virtuous.

Mining is largely involved in waste and by-products generation, globally making over 100 billion of tons of solid material in the form of rock fragments each year [2]. Therefore, applying these materials in new technological fields will mean revaluing waste and by-products that are currently difficult to manage. Pumice scraps are a clear example.

Pumices are aluminosilicate rocks with a volcanic origin, mainly composed of feldspars, quartz, cristobalite, mica, and varying amount of glass, which may constitute up to 80–90 wt% of the material [3–5]. The porous structure of pumices results from the degassing of volatile compounds and rapid expansion, leading to rocks with low bulk densities [6,7]. Pumices are primarily used for scouring, scrubbing, and as polishing material. However, debris smaller than 3 mm is largely unsold and is therefore considered a by-product. Moreover, while it is partially used to fill quarry voids, the excess must be stored in the mining area as a waste, constituting additional costs for mining companies [8–11].

Many attempts have been made to find application for pumice scraps. Fine aggregates have proved to be a promising alternative to sand in the production of lightweight cement mortar [12]. The incorporation of pumice into the cement matrix has been shown to improve thermal and acoustic insulation, as well as resistance to fire, abrasion, and degradation from prolonged contact with seawater; however, this resulted in decreased mechanical strength of the cement [13]. The potential of pumices for water and wastewater treatment has only recently been recognized by the scientific community. Indeed, natural or suitably modified pumice, have been successfully used for removing heavy metals from aqueous solutions. Pumice has proven to be efficient in coagulation and flocculation processes for removing hydrocarbons from refinery wastewater [14], and it has substantially reduced the biological

* Corresponding author.
E-mail address: giulio.galamini@unimore.it (G. Galamini).

https://doi.org/10.1016/j.micromeso.2025.113704
Received 19 November 2024; Received in revised form 24 April 2025; Accepted 21 May 2025
Available online 22 May 2025

Abbreviations

CHA	CHAbazite-rich zeolitized tuff
Mn^{2+}-EC	Mn^{2+} enrichment capacity of the materials. Namely, a fraction of the t.CEC which is available for Mn^{2+} (mmol (+)Mn^{2+} g^{-1})
Mn^{2+}-sat	Percentage of the t.CEC available for Mn^{2+} enrichment (%)
PUM	Pumice scraps
t.CEC	Theoretical cation exchange capacity. The maximum exchange capacity of the materials, measured by complete displacement of the exchangeable cations (mmol(+) g^{-1})

and chemical oxygen demand (BOD and COD, respectively) of municipal wastewaters [15].

The presence of small amount of minerals belonging to the zeolite family has been linked to the reactivity of some pumiceous materials toward specific chemical species, and their adsorption properties. Zeolites are aluminosilicates composed of structural $[SiO_4]^{4-}$ tetrahedra arranged in a three-dimensional framework that forms a microporous structure of interconnected channels and cages [16,17]. Due to the partial substitution of Si^{4+} with Al^{3+} in the tetrahedra, the resulting $[AlO_4]^{5-}$ provide zeolites with net negative surface charges, which are weakly balanced by loosely bound cations. This characteristic imparts several properties to zeolites, such as high cation exchange capacity (CEC), molecular sieving and reversible hydration. CEC is arguably the most well-known and exploited property of zeolites, allowing cations in aqueous solutions to diffuse from the external environment into the extraframework spaces, while cations originally present on the internal surfaces diffuse outward [18–22].

Zeolites are found in both hydrothermal and diagenetic environments, but economically viable deposits are primarily associated with diagenetic deposits [23,24]. Despite the possible presence of significant amounts of zeolites in pumiceous rocks that have undergone diagenetic processes – sometimes reaching up to 15 wt% [4,5,8,15,25] – these minerals are more commonly and abundantly found, occasionally over 50 wt%, in diagenized volcano-sedimentary deposits, which are generally referred as zeolitized tuffs [21,23]. The CEC of zeolitized tuffs depends not only on the amount and zeolitic species present (the primary ones in diagenetic environments are chabazite, phillipsite, clinoptilolite, and mordenite), but also on other properties such as grain size, porosity and the presence of non-zeolitic phases. As a result, zeolitized tuffs are used in various fields of application, including wastewater treatment, construction, gas adsorption, moisture and odour control, and agriculture [6,12,19–21,26–30].

Agricultural applications are receiving increasing interest. When added to soil as an amendment, zeolitized tuffs may increase soil water-holding capacity, potentially counteracting drought stress and related damage in plants [23,24,31–38]. Zeolitized tuffs suggested to decrease fertilizer-related CO_2 emissions from agricultural soil [39]; moreover, zeolites enriched with NH_4^+-N from livestock waste, used as soil amendment have shown reduced leaching compared to traditional organic and synthetic N- fertilizers ([40–43], 2022; [33,44]). N-enriched zeolite also temporarily altered the soil pH, resembling a liming effect with potentials for nutrient mobilization [42].

Another application of natural zeolitized tuffs, when finely ground to powder, is their use as foliar coaters [31,45–52]. For instance, in cases of micronutrient deficiencies, zeolitized tuffs may be enriched in micronutrients and sprayed on plant leaves, acting as a foliar corroborant potentially outperforming conventional products due to their better resistance to rain leaching [4,5]. Foliar treatments with powdered zeolitized tuffs proved also effective against pathogenic insects, namely the olive fruit fly (*Bactrocera oleae,* Rossi 1790) in olive groves [53]. In wastewater treatment, zeolitized tuffs have been used in combination with struvite precipitation technology to recover N, P, and K from livestock and industrial effluents, therefore obtaining valuable fertilizers [4,5].

Due to the aforementioned wide range of applications, solid by-products generated from zeolitized tuffs quarrying is generally negligible. However, as previously discussed, this cannot be said for pumice deposits, for which it is necessary to investigate new fields of application. Therefore, in this study we evaluated pumice by-product for Mn^{2+} enrichment from aqueous solutions and investigated its release capacity in simulated soil water to assess its potential use as a plant biofortifying. The activity of pumice scraps, with respect to Mn^{2+}, was compared with that of a more well-known and applied zeolitized tuff. Manganese has been chosen because it is an essential micronutrient for plants, and the possible slow release by the Mn^{2+}-enriched pumice and Mn^{2+}-enriched zeolitized tuff hold potential for agricultural applications.

Moreover, Mn plays a critical roles in soil ecosystems. In fact, Mn is directly involved in plant litter decomposition and soil organic carbon cycling, as demonstrated by recent studies (e.g., Ref. [54]). It has been shown that the addition of Mn accelerates the decomposition of organic substrates, increasing soil respiration (microbial-driven CO_2 emissions), as well as the transformation of organic carbon from plant residues into protected carbon within mineral-associated organic matter [55]. Nitrogen fertilization may increase soil acidity after long-term applications, thereby enhancing the bioavailability of Mn and other micronutrients in the soil, with significant effects on microbial activity and carbon cycling processes; however, intensive fertilization regimes may lead to soil Mn depletion toward the subsoil [56]. Mn can also influence soil structure. Indeed, certain bacteria have been shown to play a key role in catalysing the oxidation of Mn(II) to Mn(III) and Mn(IV), contributing to the formation of soil aggregates stabilized by Mn oxide binders [57].

Mn is present in biostimulants mainly in the form of $MnSO_4{\cdot}H_2O$, a soluble form that provides readily available Mn^{2+}. When soluble Mn^{2+} is provided through soil fertilization, excessive availability may either exceed roots absorption capacity or lead to plant toxicity, potentially interfering with the absorption of other essential nutrients and causing oxidative stress [58,59]. The main disadvantage of applying Mn directly to the soil, in fact, is the tendency to precipitate in insoluble forms, especially in alkaline soils, where free Mn is represented by cationic species prone to precipitation as Mn^{3+} and Mn^{4+} [58]. For these reasons, foliar fertilization and the use of products that ensure slow release are commonly adopted.

One of the most widely used product is manganese ethylenediaminetetraacetate (Mn-EDTA). In this compound, Mn is chelated by EDTA, forming a stable complex which ensures slow release, as well as greater Mn bioavailability in limited soils, as highly alkaline and calcareous soils [60]. Another important feature of Mn-EDTA fertilizer is the reduced risk of leaching [61]. However, there are also significant disadvantages. Mn-EDTA, as well as EDTA fertilizers in general, are expensive (i.e., 20–22 € kg^{-1} for Mn-EDTA, compared to approximately 6€ kg^{-1} for $MnSO_4$). Moreover, the prolonged use of synthetic chelators can have long-term negative effects on the soil by binding other essential micronutrients, therefore altering nutrient balance in soils [62]. Finally, the efficacy of Mn-EDTA may also be limited in very acidic soils or in the presence of competing ions [63].

With the aim of finding an alternative to the currently used Mn-based agricultural products by involving the recycling of quarry material, this research investigated the possibility of reusing pumice-based quarry by-product for the formulation of a particulate Mn-fertilizer with potential for slow release, comparing it with a more studied zeolitized tuff. Based on this premise a pumice by-product and a chabazite rich zeolitized tuff were selected and comparatively analysed. Micronized forms were investigated, therefore potentially useable in spraying machines i.e., for foliar treatments.

The theoretical cation exchange capacities (t.CEC; mmol(+) g^{-1}), namely the maximum achievable CEC, were measured by complete displacement of the exchangeable cations. The t.CEC were then compared with the respective Mn^{2+}-enrichment capacity (Mn^{2+}-EC), therefore the fraction of t.CEC available for Mn^{2+} under the experimental conditions, to estimate absolute and relative efficiencies in Mn^{2+} enrichment from a liquid solution of $MnSO_4{\cdot}H_2O$. Kinetic modelling and equilibrium isotherms were assessed with respect to Mn^{2+} enrichment, allowing the definition of optimal operating conditions for the process. To evaluate the slow-release potential of the materials, kinetic tests were conducted on the Mn^{2+}-enriched pumice and zeolitized tuff in simulated groundwater, therefore representing a typical irrigation water used in agricultural sprayer machines i.e., in foliar treatments.

We also provide a preliminary cost outlook, by comparing Mn-fertilizers with the investigated pumice and zeolite formulations.

2. Materials and methods

2.1. Materials characterization

The chabazite-rich zeolitized tuff (CHA) and pumice (PUM) were sourced from quarries in Tessennano (Viterbo, Italy). The mineralogical composition was determined using a Philips X'Pert PRO diffractometer (Panalytical, Malvern, UK) equipped with a first-generation Real Time Multiple Strip detector. Main experimental conditions were: Incident beam, Cu Kα radiation at 40 kV and 40 mA; Soller slits, 0.02 rad; anti-scatter and divergence slits, 1/4°. Diffracted beam: anti-scatter mask, 5.0 mm; Soller slits, 0.02 rad; integration time, 240 s in continuous scan (length of 2.12 °2θ corresponding to a step size of 0.0170 °2θ per s). Measurements were collected in the range 5–90 °2θ. Quantitative phase analyses were performed using the Rietveld method with the GSAS software and EXPGUI graphical interface, following the protocol reported in Ref. [64]. NIST SRM 676a (alumina powder, corundum structure) served as the internal standard and for instrument calibration. The chemical compositions were measured in electrically fused samples obtained with an xrFuse (Xrf Scientific, Australia) with an XRF (Zetium, Panalytical) sequential wavelength dispersive spectrometer (WDS), operating under vacuum conditions and equipped with 3 kW Rh tube and 5 analyzer crystals (LiF220, LiF200, Ge, PE, PX1). The quantitative phase analysis and the chemical compositions of CHA and PUM are reported in Table 1.

The potential release by CHA and PUM of elements possibly critical for plant is reported in Table 2. Leaching was evaluated in ultrapure water and 0.01 M $CaCl_2$ solution by soaking 6 g of PUM or CHA powder in 100 mL of extractant (6 % dosage, m:v) under continuous stirring at 400 rpm for 24 h. The extracts were filtered with ashless filter paper (Whatman, Maidstone, UK). The resulting clear solutions were analysed by ICP-OES (Optima 4200 DV, PerkinElmer, Waltham, MA, USA) using a calibration curve in the 0.1–20 ppm range.

Table 1
Mineralogical and chemical composition of CHA and PUM.

Mineralogical composition (wt%)			Chemical composition (wt%)		
	CHA	PUM		CHA	PUM
analcime	–	0.80 (6)	LOI	10.1	6.01
chabazite	46.8 (5)	–	SiO_2	53.8	56.2
sanidine	21.4 (3)	4.8 (2)	Al_2O_3	18.2	19.5
orthoclase	–	2.4 (1)	Fe_2O_3	3.66	3.87
phlogopite	2.5 (1)	–	MnO	0.10	0.14
muscovite	–	4.5 (1)	MgO	1.68	0.69
other	29.3 (5)	87.5 (2)	Na_2O	0.68	2.46
			TiO_2	0.53	0.57
χ^2	16.40	1.526	K_2O	5.63	7.63
R_{wp}	0.0615	0.0447	P_2O_5	0.12	0.11
R_p	0.0432	0.0349	CaO	5.23	2.53

In the mineralogical analyses: i) the standard deviation σ_Q (values in parenthesis) of the weight percent of each phase (Q) was calculated from the values obtained in the output file after the refinement by GSAS software, and the formula $\sigma_Q = \{[(\sigma_a\ a^{-1})^2 + (\sigma_b\ b^{-1})^2]^{1/2}\}\ Q$ [65], where *a* and *b* are the two variables most affecting Q values and refer, respectively, to the weight fraction of the phase and the internal standard, whereas σ_a and σ_b are their standard deviations; ii) "other" identifies phases that are either undetectable because too small in quantity, or non-crystalline phases. In the chemical analyses LOI refer to the Loss On Ignition, namely the weight loss (%) at 1050 °C.

2.2. Characterization of Mn^{2+} enrichment

The degree of Mn^{2+} enrichment in CHA and PUM was tested in a batch of 0.5 $MnSO_4$-H_2O solution, at 6 % dosage (m:v, namely 12 g in 200 mL). Samples were stirred in closed polypropylene tubes for 24 h at 400 rpm. The supernatant was then removed by centrifugation at 6000 rpm for 5 min. Powders were collected and washed 5 times with 100 mL of ultrapure deionized water (Milli-Q, Millipore, Burlington, MA, USA) to remove weakly bound and residual Mn^{2+}, then dried at 105 °C for 24 h. The Loss On Ignition (LOI) was measured in aliquots of dried samples by evaluating the percent of mass loss after calcination at 1050 °C for 3 h. The assessment of LOI is necessary as it is needed to correct the data of XRF not acquired in calcined samples. The total amount of Mn in solid samples was measured by XRF (section 2.1) and the Mn^{2+} enrichment of CHA and PUM was then calculated by the difference between total amounts in Mn^{2+}-enriched samples versus virgin samples.

Localized clusters of Mn in the materials would indicate either the presence of residual Mn from the washings, or the occurrence of insoluble Mn-precipitates. Both these scenarios were not desirable. Therefore, to ensure that no Mn precipitates occurred during the adsorption batch, Mn-chemical mappings were performed with SEM-EDX technique (JSM-6010PLUS/LA, JEOL, Tokyo, Japan).

The t.CEC was accessed with the ammonium acetate (NH_4Ac) method, as modified by ([66,67], p. 22171). Briefly, the exchange sites were saturated with a high-affinity cation (NH_4^+), and the displaced positive charges of exchanged cations (Na^+, Mg^{2+}, K^+ and Ca^{2+}) were then quantified in the solution with ICP-OES technique (Optima 4200 DV, PerkinElmer).

The oxidation state of Mn is pH dependent. In acidic and neutral aqueous solutions, the most stable form is Mn^{2+}. Mn solubility strongly decrease in oxidizing systems with neutral or alkaline pH [68], where it easily precipitates as oxide and hydroxides by reacting with the dissolved oxygen and $(OH)^-$. To be sure that the effects of adding CHA and PUM to the solution would be negligible on pH and thus on the possible precipitation of insoluble species, a 6 % dose (m:v) of CHA or PUM (12 g in 200 mL) was mixed with a magnetic stirrer, in contact with a 0.5 M $MnSO_4{\cdot}H_2O$ solution, and the pH was monitored at 1, 30, 150 and 240 min of contact, with an Orion 9102BNWP pH-meter (Thermo Fisher Scientific, Waltham, MA, USA).

2.3. Adsorption kinetic, isotherms and Mn^{2+} release

In the adsorption kinetic tests, a 15 % dose (m:v) of CHA and PUM was used. Specifically, 6 g of each material were added to 40 mL of

Table 2
Release of possibly undesirable cations from CHA and PUM (mg kg^{-1}).

	Releasable fraction in water		Releasable fraction in 0.01M $CaCl_2$	
	CHA	PUM	CHA	PUM
Na	45.5	37.5	43.8	31.3
Al	1.7	0.4	1.0	0.2
V	1.3	<0.1	0.8	<0.1
Cr	<0.1	<0.1	<0.1	<0.1
Co	<0.1	<0.1	<0.1	<0.1
Ni	<0.1	<0.1	<0.1	<0.1
As	<0.1	<0.1	<0.1	<0.1
Cd	<0.1	<0.1	<0.1	<0.1
Pb	<0.1	<0.1	<0.1	<0.1

$MnSO_4 \cdot H_2O$ solution containing 1000 ppm of Mn^{2+}. Samples were closed in polypropylene tubes and mixed with an orbital shaker at 400 rpm. The supernatant was then separated from the solution at 5, 10, 15, 30, 45, 60, 100, 130 min, and 14 h, which was assumed as close to the equilibrium.

Adsorption isotherms were investigated using the same batch volume (40 mL) and mixing rate (400 rpm) as in the kinetic tests, but with different masses of CHA and PUM: 1, 2, 3, 4, 5, 6, 7, 9, 11, 13 and 15 g. Equilibrium was assumed to be reached after 24 h of contact, at which samples were collected.

The kinetics of Mn^{2+} release from the Mn^{2+}-enriched CHA and PUM were evaluated. To simulate agricultural applications (foliar film technology), a synthetic groundwater was used, designed to mimic the properties of water used with spraying machines. Therefore, to prepare the synthetic groundwater, the following reagents were used, with concentrations (mg/L) indicated in parentheses: $CaSO_4 \cdot 2H_2O$ (150), NaCl (150), $NaHCO_3$ (250), $MgSO_4 \cdot 7H_2O$ (500), KNO_3 (13), $MgCl_2$ (65), $CaCl_2$ (100). The resulting concentrations of dissolved ions were consistent with the composition of real non-saline groundwaters [69, 70], namely (mg L^{-1} in parentheses): Ca^{2+} (71), Mg^{2+} (43), Na^{+} (127), K^{+} (5), SO_4^{2-} (224), Cl^{-} (178), HCO_3^{-} (182), NO_3^{-} (8).

CHA and PUM used in the desorption tests were previously enriched in Mn^{2+} as described below. A 13 % dosage (m:v) was added to a $MnSO_4 \cdot H_2O$ solution containing 1000 ppm of Mn^{2+} and mixed at 400 rpm with an orbital shaker for 180 min, which, according to the results of the kinetic tests (Section 3), was sufficient to reach near equilibrium. Afterward, CHA and PUM were allowed to decant for 24 h and then separated using a vacuum filtration system consisting of a Buchner funnel with Whatman filter paper on top. Suction was provided by a water-jet vacuum pump connected to a tailed flask as a receiver. CHA and PUM were then washed twice by mixing approximately 200 g (dry weight) of each with 2 L of ultrapure deionized water (Milli-Q, Millipore), stirred with a magnetic stirrer for 30 min and separated using the same vacuum filtration system. The effectiveness of the washes in removing the reagent remained in solution ($MnSO_4 \cdot H_2O$) was evaluated by comparing the sulfur content in virgin versus treated samples through XRF measurements, which showed negligible differences.

Desorption kinetics were investigated by preparing polypropylene tubes containing 3 g of Mn^{2+}-enriched CHA or PUM and 50 mL of simulated groundwater (6 % dosage, m:v). The samples were mixed at 400 rpm with an orbital shaker, and aliquots were collected at various time intervals: 15, 30, 60, 120, 180, 240, 360 min; 1, 2, and 5 days.

For all the tests described in this section, dissolved Mn^{2+} was measured in liquid samples collected and separated from CHA and PUM through filtration with Whatman ashless filter paper, followed by filtration with nylon syringe filters (0.2 μm in diameter). Each sample consisted of 10 mL of simulated groundwater, acidified with 100 μL of 65 % HNO_3. The concentration of dissolved Mn^{2+} was measured by ICP-OES (Optima 4200 DV, PerkinElmer). Modelling was carried out using R Studio [71], with isotherm and kinetic modelling performed using the PUPAIM [72] and PUPAK [73] packages, respectively.

The Mn enrichment was also evaluated in selected solid samples of CHA and PUM, to monitor the mass balance and assess any potential Mn loss during the enrichment process.

3. Results and discussion

3.1. Efficiency of materials in Mn^{2+} enrichment

The Mn present in virgin CHA and PUM is 0.077 and 0.11 % (m:m; calculated from the MnO values in Table 1). The treated materials, which have a Mn content of 0.83 and 0.42 % for CHA and PUM, respectively, thus exhibit an enrichment of about ten and three times compared to virgin materials. The greater enrichment of CHA with respect to PUM is consistent with its higher zeolite content.

The amount of Mn in CHA was approximately two times higher than PUM. Therefore, to obtain the same application in agricultural use, it should be required about double the amount of PUM with respect to CHA. However, it should be considered that plant effects are not related to total amount of Mn, rather to the releasable (phytoavailable) fraction.

As outlined below, the enriched PUM showed higher capacity of releasing Mn than the enriched CHA (section 3.4). Indeed, the release of Mn^{2+} by PUM at equilibrium is approximately 1.5 times higher than that of CHA (section 3.4). Therefore, to obtain with the enriched PUM the same amount of released Mn available for plant biofortification, it is necessary less material than CHA. In addition, using less material to achieve the same result also results in fewer potentially agronomically undesirable elements (Table 2).

PUM has a t.CEC approximately one order of magnitude lower (0.173 vs. 1.487 mmol(+) g^{-1}) compared to CHA (Table 3). However, PUM demonstrated a higher affinity for Mn^{2+} compared to CHA, as indicated by the percent of saturation (Mn^{2+} sat.), which represent the percentage of the t.CEC (charge density) that can be occupied by Mn^{2+} charges (Table 3). As described in section 2.2, this parameter was derived by saturating the materials with 0.5 M $MnSO_4 \cdot H_2O$. While Mn^{2+} sat. Was approximately 18 % in CHA (therefore, 18 % of the exchangeable charges were represented by Mn^{2+}), it reached 65 % for PUM. Thus, despite its lower CEC, PUM exhibited nearly four times greater affinity for Mn^{2+} than CHA.

The active mineral present in PUM is analcime, belonging to the zeolite family, and is present at 0.80 wt% (Table 1). Considering that the CEC of analcime is approximately 4.5 mmol(+) g^{-1} [74], the expected CEC contribution from analcime alone would be about 0.036 mmol(+) g^{-1}, which is significantly lower than the measured t.CEC (approximately 0.17 mmol(+) g^{-1}). Therefore, it is plausible that the detectable zeolites in pumice contributed minimally to the overall activity regarding Mn^{2+} and CEC, suggesting that active sites for Mn^{2+} may have been present in other phases of PUM, likely including the amorphous fraction, of the material, which constituted the majority of PUM (Table 1).

Regarding the effect on the pH of the $MnSO_4 \cdot H_2O$ solution (section 2.2), CHA and PUM increased the pH from the initial value of 5.73, to 6.25 and 6.30, respectively, after 240 min of contact. This increase was likely due to the release of alkaline counterions such as Na^{+}, Mg^{2+}, K^{+} and Ca^{2+}. At room temperature, Mn^{2+} is coordinated by 6 water molecules, and the initial pH of 5.73 in a 0.5 M $MnSO_4 \cdot H_2O$ solution results from the speciation of dissolved Mn^{2+} into two singly charged cations through hydrolysis of water in the hydration shell [75]: $Mn^{2+}(H_2O)_6 \rightarrow MnOH^{+}(H_2O)_5 + H^{+}$ where $Mn^{2+}(H_2O)_6$ is the hydration shell in octahedral coordination. At 240 min of contact, equilibrium for pH was not yet been reached; however, between 180 and 240 min, the increase was less than 1 %, suggesting that a condition close to equilibrium was achieved. Nevertheless, the pH was always lower than 7, with the highest value measured in PUM at 240 min (6.30), therefore no Mn-precipitates were expected. To validate this hypothesis, semi-quantitative chemical analyses were conducted using SEM-EDS

Table 3
Amount of exchangeable (exch.) cations by CHA and PUM (mmol(+) g^{-1}) and fraction of the CEC available for Mn^{2+} (%).

	exch. Na^{+}	exch. Mg^{2+}	exch. K^{+}	exch. Ca^{2+}	t.CEC	Mn^{2+}-EC	Mn^{2+} sat
	mmol(+) g^{-1}						%
CHA	0.037	0.070	0.402	0.977	1.487	0.273	18.4
PUM	0.001	0.022	0.061	0.089	0.173	0.113	65.2

The t.CEC is the theoretical cation exchange capacity, equal to the sum of the overall exchangeable positive charges of the counterions per g of material (mmol(+) g^{-1}). Mn^{2+}-EC is the enrichment capacity of the materials under saturation with 0.5 M $MnSO_4 \cdot H_2O$. Mn^{2+} sat. Represent the percentage (%) of the t.CEC available for Mn^{2+} enrichment, namely the maximum enrichment in Mn^{2+} achievable by the materials under the experimental conditions.

technique on the Mn^{2+}-enriched materials, as described in section 2.2. No Mn clusters were observed in the materials, except for a few small, localized areas in CHA (Fig. 1A and B) that were also associated with Ti and/or Fe (Fig. 1C and D). The simultaneous presence of Ti and Fe indicates that these phases were already present in the original sample, and the flat morphology of the observable fragment in the lower right part of Fig. 1A suggests that it is a phlogopite crystal, in agreement with mineralogical analyses (Table 1). However, it cannot be ruled out that clusters with this chemical composition are also present in the amorphous fraction without however affecting the results obtained.

Concerning the mechanisms involved in Mn^{2+} adsorption, the predominant process in CHA was cation exchange, due the high zeolite content. In zeolites, cation exchange occurs at specific sites with a permanent negative charge. Active sites arise because of the isomorphic replacement of Si^{4+} with Al^{3+} in the mineral framework, resulting in net negative charges [16]. Cations as Na^{+}, Mg^{2+}, K^{+}, and Ca^{2+} balance the electrical charges, providing electrical neutrality, but can be involved in exchange reactions with surrounding counterions. The reaction, which is commonly reversibility, could be represented as shown below:

$$\equiv X\text{–}Y^{n+} + Z^{n+} \rightleftharpoons \equiv X\text{–}Z^{n+} + Y^{n+} \quad (1)$$

where ≡ X indicates a structural site with a permanent negative charge (i.e., ≡Al–O) or multiple adjacent sites, Y is the exchangeable cation, and Z is the counterion.

Other minor mechanisms of cation exchange in zeolites involve the occurrence of silanol (Si–O–H) and hydroxyl groups attached to Al in the edge of the crystal (≡Al–OH), and located in the terminal parts of zeolites as edges, faces and along faults [76].

Cation exchange was likely relevant also in PUM, partly due to the presence of zeolites with high-CEC (analcime). However, it is likely that the amorphous fraction (volcanic glass) provided the major contribution to the CEC [77,78].

Pumices exhibit negative zeta potential values over a broad range of pH, and the mesoporous structure of pumices offer large specific surface area [79]. Industrial grinding play also a key role in increasing the activity of pumices. Several studies have demonstrated that the chemical reactivity of pumice increases significantly through mechanical milling, which enhances the amorphous (reactive) component at the expense of crystalline phases (e.g., Ref. [80,81]). The employed material undergone mechanical milling in the cave. Its also showed remarkable specific surface area (18.005 ± 0.099 m^2/g; [4,5]). Taken together, the overmentioned aspects (mechanical activation, high specific surface area, and the presence of negatively charged surfaces throughout the entire pH range under investigation) may explain the reactivity of pumice toward Mn^{2+}.

3.2. Kinetic of Mn^{2+} enrichment

Once it was assured that Mn-precipitates were absent, it was investigated the enrichment of Mn^{2+} by CHA and PUM through kinetic and equilibrium tests (section 3.3). For the kinetic investigations, it is advisable to avoid linearized models, as they can often induce statistical biases [82]. Additionally, data points close to equilibrium (i.e., when $q_t \approx q_e$) should be avoided as well. This is particularly relevant in the context of the frequent misuse of the Pseudo-Second-Order (PSO) model compared to the Pseudo-First-Order (PFO), as highlighted by Ref. [83]. Therefore, kinetic modelling was calculated using only data with a fractional uptake F(t), defined as $F(t) = q_t\, q_e^{-1}$, that was equal to or less than 0.95.

F(t) indicated a slower enrichment for CHA compared to PUM. Specifically, PUM reached an $F(t) \geq 0.85$ after just 5 min of contact with $MnSO_4{\cdot}H_2O$ solution, whereas CHA took 1 h to reach $F(t) \geq 0.85$. Therefore, from a practical standpoint, PUM can be maintained in batch suspension for a few minutes to achieve a good enrichment in Mn^{2+}, while CHA requires a longer duration. In PUM, the rapid initial kinetic of Mn^{2+} enrichment, combined with the high Mn^{2+}-sat previously discussed (section 3.1), indicates a higher affinity of PUM for Mn^{2+} ions compared to CHA. Conversely, the adsorption capacity (q; mg Mn^{2+} g^{-1}) of CHA was approximately 1.4 times greater than that of PUM, likely due

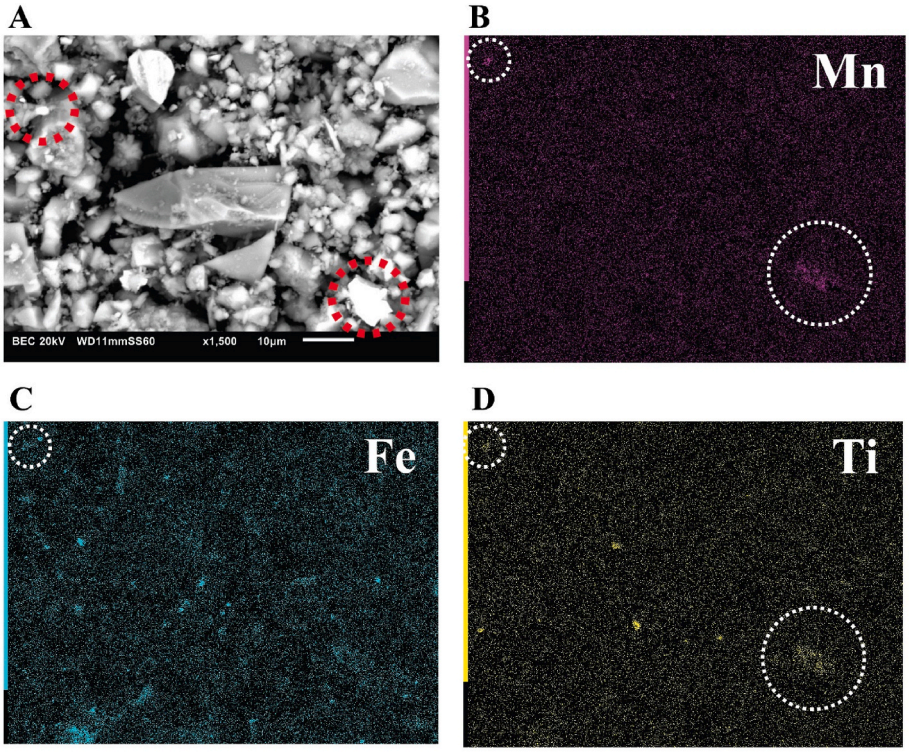

Fig. 1. SEM-EDS imaging of the Mn^{2+}-enriched chabazite zeolitized tuff (CHA). A) Backscattered electron scanning of CHA, and map distribution of Mn (B), Fe (C) and Ti (D). Dotted lines mark localized regions with slightly greater concentration of Mn, in association with Ti and/or Fe.

to its higher content of zeolite minerals, specifically chabazite (Table 1).

CHA exhibited strong correlations with the Weber-Morris Intraparticle diffusion and Elovich models (Table 4; Fig. 2B and C). The Weber-Morris model is expressed in Eq. (2) [84]:

$$q_t = k_{ID}\sqrt{t} + C \quad (2)$$

where k_{ID} (mg g^{-1} × $min^{1/2}$) is the kinetic rate constant, and C (mg g^{-1}) is a constant associated with the resistance to diffusion. Weber-Morris Intraparticle diffusion is a multi-linear process in which intraparticle diffusion limits adsorption or exchange. Each line has its own k_{ID} and C value, with higher C indicating a greater thickness of the boundary layer that hinders the diffusivity of the chemical species (in this case, Mn^{2+}) within the porous structure of the material (in this case, zeolite mineral). Consequently, the mass transfer of Mn^{2+} within the porous structure of chabazite in CHA was likely limited by diffusion kinetic, which was not the case for PUM. In CHA, two distinct stages were observed; the second began around 2 h of contact (as shown by the line on the right in Fig. 2C), where the diffusion through the boundary layer gradually slowed, approaching equilibrium condition. The first line had a C value of 2.05 mg Mn^{2+} g^{-1}, indicating that also during the first 2 h of contact with the $MnSO_4{\cdot}H_2O$ solution, enrichment was constrained by surface layer diffusion.

The Elovich model is presented in Eq. (3) [85]:

$$q_t = \frac{1}{\beta}\ln\left(1 + \alpha\beta t\right) \quad (3)$$

where α is the initial adsorption rate (mg Mn^{2+} g^{-1} s^{-1}) and β is a constant related to the extent of the surface coverage. Elovich kinetic is an empirical model which is commonly used in chemisorption; however, it has also been identified as a good predictor for the adsorption of heavy metals by clay minerals [86] and zeolites [87].

3.3. Isotherm models

Two distinct behaviours were observed in CHA and PUM (Fig. 3A). As expected, CHA achieved higher q_e values compared to PUM due to the higher amount of zeolite (Table 1). The shape of the isotherm also differed, as CHA likely exhibited a type II isotherm, while PUM showed a type I isotherm [88]. The larger variation in q_e values in CHA was 2.39 mg Mn^{2+} g^{-1}, while in PUM it was just 0.43 mg Mn^{2+} g^{-1}, indicating that PUM experienced conditions of semi-saturation for each point of the model. In other words, PUM achieved nearly the same q_e regardless of the solid to liquid ratio used, which is remembered to have been applied between 2.5 and 37.5 % (w:v) in $MnSO_4{\cdot}H_2O$ at 1000 ppm of Mn. From an applicational perspective, this behaviour offers a significant advantage, as an industrial plant could utilize nearly any dosage of PUM relative to the batch volume of solution, achieving similar product characteristics in terms of Mn^{2+} enrichment. This indicates the good stability of PUM with respect to Mn^{2+} enrichment and therefore, easiness in process prediction.

The average of the measured q_e of PUM was 1.46 ± 0.18 mg Mn^{2+} g^{-1}, which was consistent with the t.CEC (1.57 mg Mn^{2+} g^{-1} = 0.173 mmol(+) g^{-1}).

While PUM exhibited slight variations in q_e, CHA demonstrated a significant increase at the rightmost part of the graph (Fig. 3A). This indicates that enrichment was facilitated by lower solid-to-liquid ratios were used. As anticipated, all q_e values for CHA were higher than those of PUM, with the maximum q_e recorded at 2.5 % w:v dosage (4.25 mg Mn^{2+} g^{-1}) and the minimum at 37.5 % (1.83 mg Mn^{2+} g^{-1}). In contrast to PUM, the type II shape of the isotherm of CHA compels to carefully control the solid/liquid ratio to allow accurate predictions of the enrichment in Mn^{2+}.

It was not possible to perform isotherm modelling on PUM due to the limited variation in q_e. The Harkins-Jura model showed the best correlation and significance (0 < p-value <0.001) with the experimental data for CHA (Table 5 and Fig. 3B). The model is expressed in Eq. (4) [89]:

$$q_e = \left(\frac{A_H}{B_H - \ln C_e}\right)^{1/2} \quad (4)$$

where A_H and B_H are constants, and B_H is related to the specific surface area of the material. Harkins-Jura accounts for multilayer adsorption, and is commonly applied in solids with an heterogeneous pore structure [90]. The structure of zeolites is ordered in a crystalline lattice, determining an ordered microporous structure; however, being CHA a natural material (zeolitized tuff) the presence of heterogeneous regions could be an option. For instance, the heterogeneity of the porous structure of a zeolite-rich rock (in this case, clinoptilolite) has been pointed out by Mansouri et al. [91]. Additionally, Harkins-Jura, as well as other multilayer isotherm models (i.e., Freundlich, also reported for CHA in Fig. 3B) have been demonstrated suitable for certain zeolite samples (i.e., [19,20]).

3.4. The kinetic of Mn^{2+} release

The content of Mn occurring in virgin CHA and PUM was 0.77 and 1.08 mg Mn g^{-1}, respectively (Table 1). After the batch with $MnSO_4{\cdot}H_2O$ (section 2.3), their content was 3.72 and 2.97 mg Mn g^{-1}, therefore the materials used in the release tests with the synthetic groundwater (section 2.3) had a content of likely-exchangeable Mn^{2+} of approximately 2.95 and 1.89 mg Mn g^{-1}, respectively. However, despite the

Table 4
Statistical parameters of kinetic models and constants respect to Mn^{2+}-adsorption from $MnSO_4{\cdot}H_2O$ solution for CHA and PUM.

	Models	Statistics					Kinetic constants							
		RMSE	MAE	AIC	SE	R^2	param. 1		param. 2		param. 3		param. 4	
CHA	*Avrami*	0.092	0.072	−15.2	0.102	–	k_{Av}	0.767	n	0.229	–	–	–	–
	Elovich	0.089	0.070	−16.1	0.098	–	α	$1.23{\cdot}10^{3}$	β	4.64	–	–	–	–
	Fractional Power	0.091	0.072	−15.6	0.100	–	α	0.610	β	0.080	–	–	–	–
	PFO	0.428	0.375	16.5	0.473	–	k_{PFO}	0.151	–	–	–	–	–	–
	PSO	0.256	0.222	5.25	0.283	–	k_{PSO}	0.078	–	–	–	–	–	–
	W&M ID	–	–	−20.8	–	0.957	$k_{ID}1$	0.090	C1	2.05	$k_{ID}2$	0.015	C2	2.82
PUM	*Avrami*	0.024	0.021	−26.1	0.029	–	k_{Av}	1.55	n	0.102	–	–	–	–
	Elovich	0.023	0.020	−26.8	0.027	–	α	$5.47{\cdot}10^{11}$	β	17.8	–	–	–	–
	Fractional Power	0.023	0.019	−27.0	0.027	–	α	0.799	β	0.031	–	–	–	–
	PFO	0.212	0.207	2.15	0.251	–	k_{PFO}	0.309	–	–	–	–	–	–
	PSO	0.133	0.126	−4.37	0.157	–	k_{PSO}	0.317	–	–	–	–	–	–
	W&M ID	–	–	−20.2	–	0.748	$k_{ID}1$	0.018	C1	1.75	$k_{ID}2$	0.038	C2	1.64

Avrami, Elovich, Fractional Power, Pseudo-First Order, and Pseudo-Second Order are non-linear models, while Weber-Morris Intraparticle Diffusion is linear. The acronyms of statistical parameters are: RMSE (Root Mean Square Errors), MAE (Mean Absolute Error), AIC (Akaike Information Criterion), SE (Standard Error) and the coefficient of determination (R^2), which is indicated only in the Weber-Morris intraparticle diffusion, representing the overall coefficient of determination of two distinct lines.

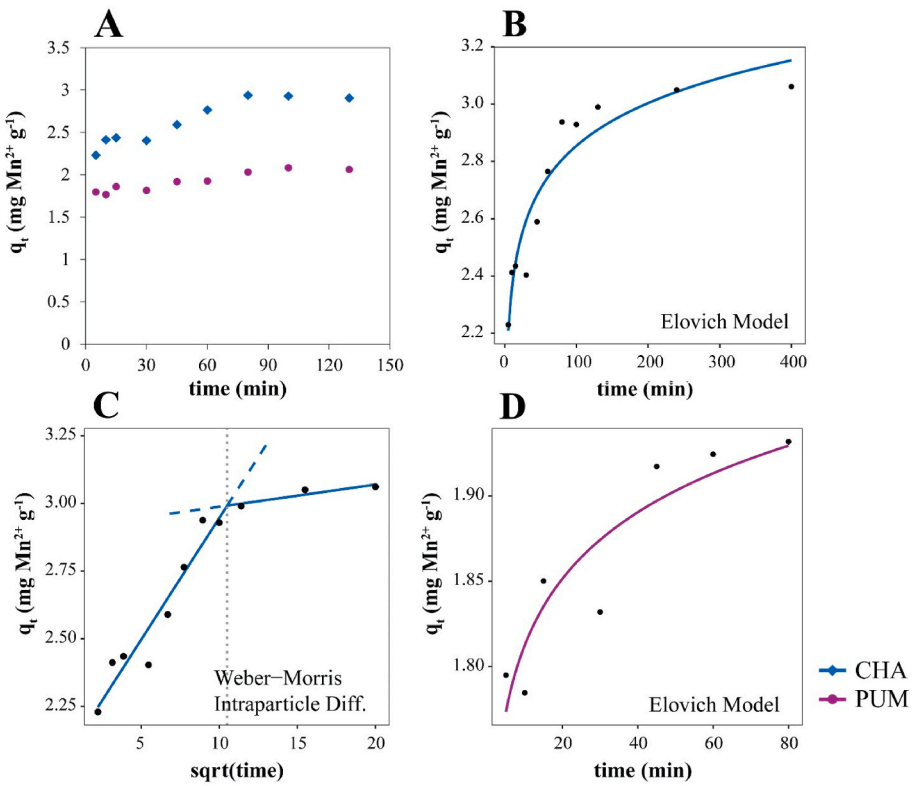

Fig. 2. Kinetic data and modelling concerning the Mn^{2+}-enrichment of CHA and PUM. A) q_t (mg Mn^{2+} g^{-1}) vs. time (min); B) Elovich kinetic model for CHA; C) Weber-Morris Intraparticle Diffusion for CHA; D) Elovich model for PUM.

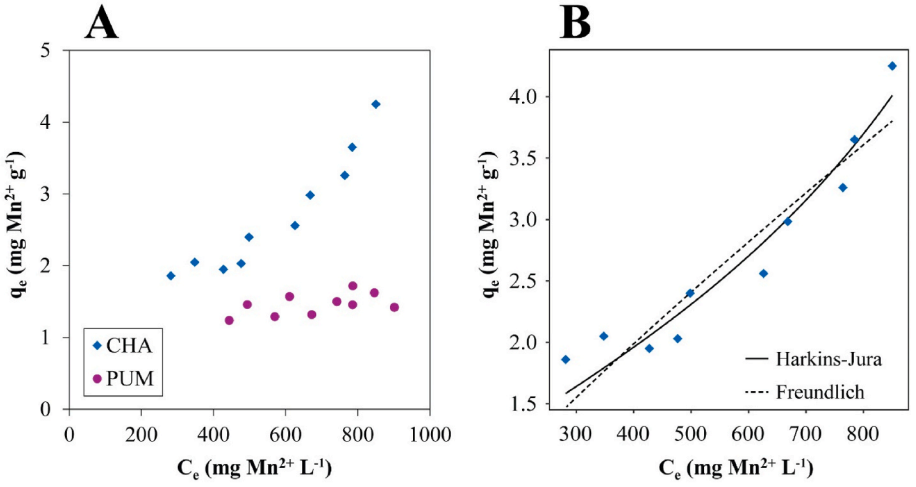

Fig. 3. Equilibrium plots. A) q_e vs C_e plot for CHA and PUM; B) Harkins-Jura and Freundlich isotherm models for CHA.

greater enrichment of CHA compared to PUM, CHA showed a lower capacity to release Mn^{2+} than PUM (Fig. 4A), whereas PUM released a higher proportion of Mn^{2+}, and showed superior release capacity ($q_{t\text{-}rel}$; Fig. 4A).

Both CHA and PUM released only a fraction of the Mn^{2+}, equal to about 13.8 and 30.4 %, respectively. By considering the composition of the synthetic groundwater, the concentration of positive charges (Na^+, Mg^{2+}, K^+ and Ca^{2+}) approximatively accounted for 12.7 mmol(+) L^{-1}. The volume of solution used in each sample was 0.05 L, therefore 0.635 mmol of positive charges, potentially exchangeable with Mn^{2+}, were present. Three g of CHA and PUM were added, contributing to 8.84 and 5.68 mg of potentially exchangeable Mn^{2+}, meaning 0.161 and 0.103 mmol(+) represented by Mn^{2+}. Therefore, the number of charges of Mn^{2+} in CHA and PUM was significantly lower than the charges present in the solution. However, it is possible that the ionic strength of the synthetic groundwater was insufficient for allowing complete exchange, that was also beyond the scope of this study, which indeed aimed at verify the release of Mn^{2+} in a realistic water intended for agricultural use.

Another difference was the fastness in the release of PUM against CHA: after 15 min, PUM reached an F(t) of 0.64 (with $q_{t\text{-}rel} = 0.346$ mg Mn^{2+} g^{-1}) while CHA had a F(t) of 0.30 ($q_{t\text{-}rel} = 0.106$). In fact, F(t), which is remembered to be equal to q_t q_e^{-1}, was initially steeper in PUM than CHA (Fig. 4B); then, CHA slowly converged to the values of PUM, reaching the same F(t) after about 25–30 h of contact with the synthetic groundwater.

Table 5
Statistical parameters and equilibrium constants for the optimal fitting isotherm models for CHA.

Models	Statistics					Equilibrium constants	
	RMSE	MAE	AIC	SE	R^2		
Freundlich	0.271	0.235	8.27	0.031	0.879	K_F = 0.0118	n = 1.17*
Harkins-Jura	0.195	0.172	1.69	0.038	0.939	A_H = 5.79*	B_H = 7.47*
Henry	0.256	0.223	7.15		0.890	K_{HE} = 0.00393	–

Statistical parameters are RMSE (Root Mean Square Errors), MAE (Mean Absolute Error), AIC (Akaike Information Criterion), SE (Standard Error) and the coefficient of determination (R^2). When * is present the p-values is between 0 and 0.001. p-value >0.05 if no * is present.

The slower diffusivity of Mn^{2+} in CHA compared to PUM, should consider both the processes involved and the characteristics of Mn^{2+} in aqueous solution at the experimental conditions. Concerning the materials, the main active fraction in CHA is chabazite (with also possible minor contribution of the amorphous fraction). The mass transfer of Mn^{2+} is a multistage process that involve internal diffusion through the microporous structure of chabazite, boundary layer diffusion, and the diffusion from the boundary layer to the aqueous solution [92]. In the case of PUM, it is likely that the most of the Mn^{2+} active sites were in the amorphous (i.e., glass) or semi-crystalline fractions, which constituted about 87.5 wt% of the material (Table 1). PUM showed greater affinity for Mn^{2+} and release capacity, however, for the purpose of this work, the adsorption and/or exchange processes were not mechanistically investigated, being the focus on the applicational perspective of PUM, simulating the environment of spraying machine tanks used in foliar fertilization.

Beside for the nature of materials, kinetic also depends on the chemical form of the Mn^{2+}. In aqueous solutions at room temperature, Mn^{2+} is coordinated by 6 water molecules, forming the Mn^{2+}-hexahydrate cation $[Mn(H_2O)_6]^{2+}$, from which monovalent cationic species are partially produced via hydrolysis of water molecules in the hydration shell, as follows: $Mn^{2+}(H_2O)_6 \rightarrow (MnOH)^{+}(H_2O)_5 + H^{+}$ [75]. Mn^{2+}, therefore, diffuses within the aqueous media by continuously exchanging water molecules with the environment, while maintaining a 6-coordination number. Nevertheless, as chlorides and $NaHCO_3$ were used to prepare the synthetic groundwater, in this study other ionic forms of Mn(II) could have developed, such as $[Mn(H_2O)_6\text{-}Cl]^{+}$ and $[Mn(H_2O)_6\text{-}HCO_3]^{+}$. In this context, the slower diffusion of Mn^{2+} in CHA respect to PUM (section 3.2), could have been related to the capacity of Mn^{2+} to form and disrupt hydrated cationic complexes and, in this case, with other anionic species present in the groundwater, in relation with the distinct nature of the materials. For both CHA and PUM, the optimal fitting kinetic models describing the release of Mn^{2+} in simulated groundwater were Elovich and Weber-Morris Intraparticle Diffusion. Statistical parameters and constants are reported in Table 6, while curves are shown in Fig. 4A–C and D.

3.5. Potential of CHA and PUM to vehiculate Mn^{2+} to crops and preliminary cost outlook

The data discussed highlight that CHA and PUM have substantially different behaviour. However, both the materials have potential for agronomic application in the case of Mn deficiencies by crops; it cannot be ruled out that their synergistic application in a combined product composed of both CHA and PUM could bring significant benefits. The fast release of Mn^{2+} by PUM could indeed cope with incipient deficiencies, while the slow release by CHA would promote maintenance of the required nutrient level by preventing damage from excessive

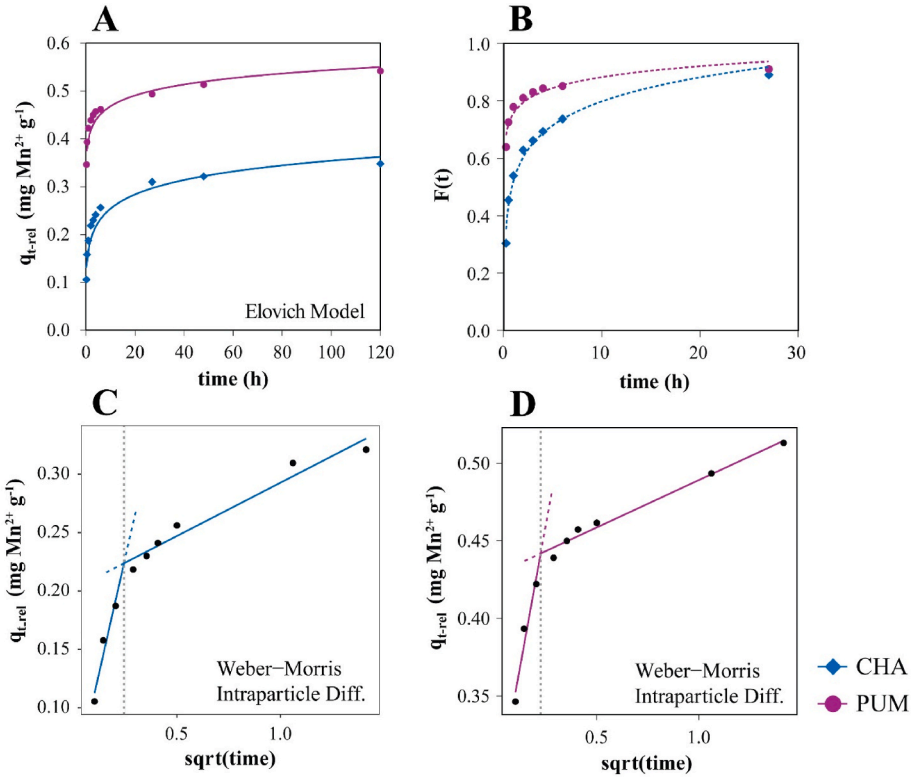

Fig. 4. Release kinetics of Mn^{2+} in simulated groundwater by Mn^{2+}-enriched CHA and PUM. A) time-dependent capacity of Mn^{2+} release ($q_{t\text{-}rel}$), namely the mass of Mn^{2+} released per gram of material at time t, against time (h). Non-linear Avrami kinetic models for CHA and PUM are shown; B) Fractional uptake F(t) against time (h). Lines are logarithm regressions and are merely used for visualizing the trends of F(t). Weber-Morris intraparticle diffusion model of CHA (C) and PUM (D) respect to Mn^{2+} desorption.

Table 6
Statistical parameters and constants of Elovich and Weber-Morris Intraparticle Diffusion kinetic models respect to the release of Mn^{2+} simulated irrigation water for Mn^{2+}-enriched CHA and PUM.

	Models	Statistics					Kinetic constants							
		RMSE	MAE	AIC	SE	R^2	param. 1		param. 2		param. 3		param. 4	
CHA	*Elovich*	0.010	0.010	−51.5	0.011	–	α	3.84	β	25.3	–	–	–	–
	W&M ID	–	–	−50.5	–	0.983	$k_{ID}1$	0.159	C1	0.033	$k_{ID}2$	0.019	C2	0.201
PUM	*Elovich*	0.011	0.009	−49.4	0.013	–	α	$53.6 \cdot 10^3$	β	35.2	–	–	–	–
	W&M ID	–	–	−59.4	–	0.988	$k_{ID}1$	0.148	C1	0.278	$k_{ID}2$	0.013	C2	0.428

Statistical parameters are as follows: RMSE (Root Mean Square Errors), MAE (Mean Absolute Error), AIC (Akaike Information Criterion), SE (Standard Error) and the coefficient of determination (R^2), which is indicated only for the multi-linear Weber-Morris model and represent the overall coefficient of determination.

accumulation. The design of such a mixture would obviously require additional study and extensive trials in the field. In support of this consideration, previous studies showed that similar materials are capable of slow-release of nutrients when employed for foliar treatments [4,5,31,48,51,52,93] and in the soil [33,39–44].

Pumice by-products are mostly reused for rehabilitation of quarry areas, but with additional costs for transportation. Pumice scraps can also be stored in inland landfills, paying a fee when resold (Directive 2008/98/EC, 2008; DL 152/2006, 2006; DPR 120/2017, 2017).

Below is a preliminary cost analysis of PUM- and CHA-based fertilizers enriched with Mn^{2+} compared to currently available commercial Mn-products. The analysis refers mainly to the European market, where countries such as Italy, Spain, and Germany represent some of the main consumers of foliar fertilizers.

The cost of Mn-based foliar fertilizers depends on the formulation. Typically, average prices range from 10 to 22 € L^{-1}, with some products reaching up to 50 € L^{-1} for Mn-EDTA. This wide range of prices depends on the quality of the raw materials and the production processes employed. The cost of $MnSO_4$, one of the most common forms of Mn in agricultural products, is approximately 6 € kg^{-1}. To estimate a plausible cost for the formulation, the costs of raw materials and energy consumption are considered.

Natural zeolites and pumice show highly variable prices depending on the particle size. Zeolitized tuff costs approximately 0.15 € kg^{-1} for a particle size of 0–6 mm and about 1.65 € kg^{-1} for particles smaller than 20 μm. Since the fine fraction (<3 mm) of pumice is currently considered a by-product of quarrying activities, its cost is even lower than that of zeolitized tuff. Pumice is priced at 0.015 € kg^{-1} for 0–6 mm particles and 0.75 € kg^{-1} for particles smaller than 20 μm. Formulation energy consumption is estimated at 6–7 € kg^{-1}.

Given the aforementioned considerations, the Mn-based product proposed would still be competitively priced, especially compared to Mn-EDTA products, which typically start at 20–22 € kg^{-1}.

4. Conclusions

Soil manganese deficiency can lead to plant diseases and reduced yields, making it essential to provide manganese to crops in certain situations. To revalorize difficult-to-manage mining by-products, this study proposes a potential manganese fertilizer based on pumice scraps, aiming to address both efficient plant nutrition by slow release and the disposal of problematic quarry by-products. Although this research certainly needs to be complemented with field trials (e.g. to ascertain possible phytotoxicity), it explored the potential use of the materials investigated (especially pumice) by providing kinetic models and adsorption isotherms and offering a preliminary cost estimate for a hypothetical Mn^{2+}-enriched pumice corroborant.

Pumices, often viewed as inert in the market, may serve as a valuable resource for supplying manganese to crops through foliar fertilization. This process involves removing the metal from aqueous solution and subsequently releasing it onto plant leaves. Compared to the zeolitized tuff used, pumice demonstrated a greater affinity for manganese, exhibiting a higher saturation percentage of the cation exchange capacity, a faster enrichment, and quicker release in simulated groundwater. Although the overall enrichment of pumice was lower, the amount of manganese released was significantly higher, suggesting the potential of using less pumice in agricultural applications, compared to the zeolitized tuff, while achieving comparable results in terms of manganese phytoavailability. Both manganese-enriched zeolitized tuff and pumice hold potential for slow-release applications, and they may be combined to formulate mixtures with suitable release kinetics, allowing for immediate release to meet urgent plant needs, followed by gradual release.

Substances commonly applied, such as $MnSO_4$, have been shown to have potential negative effects on crops, including leaching from leaves and localized phytotoxicity. If these salts were used to enrich pumice for foliar treatments, the mother liquors could be reused multiple times in sequential adsorption batches. This would result in a gradual depletion of Mn and an enrichment in Ca, K, Mg, and trace amounts of Na. Once "exhausted," these manganese-rich solutions, with Ca, K, and Mg, could also be potentially used as foliar treatments, either in liquid form or as a dry residue.

CRediT authorship contribution statement

Giulio Galamini: Writing – original draft, Methodology, Investigation, Formal analysis, Data curation, Conceptualization. **Altimari Fabiana:** Writing – original draft, Visualization, Formal analysis. **Barbieri Luisa:** Writing – review & editing, Supervision, Resources, Funding acquisition, Conceptualization. **Malavasi Gianluca:** Visualization, Resources, Conceptualization. **Malferrari Daniele:** Writing – review & editing, Supervision, Resources, Funding acquisition, Formal analysis, Conceptualization.

Funding

This work was funded under: i) the PNRR-M4C2INV1.5, NextGenerationEU-Avviso 3277/2021-ECS_00000033-ECOSISTER-spk1; ii) PRIN2022 “SEEDS - Sediments Eco-recycling Exploitation, Development and Sustainability” – Project Code 2022BCL34N, funded by the European Union (EU) - Next Generation EU, Missione 4 Componente 1 CUP-E53D23004330006. iii) UNIMORE PhD course in “Industrial and environmental engineering” 2021/22 with one place with scholarship with topic “Volcanic minerals for the green transition (VolMin4GT): Valorization and eco-sustainable recovery of volcanic and melting minerals, and related scrap” (Action IV.5 "Doctorates on green thematics” within National Operational Programme on Research and Innovation 2014–2020).

Declaration of competing interest

The authors declare that they have no known competing financial interests or personal relationships that could have appeared to influence the work reported in this paper.

Acknowledgements

We gratefully thank Davide Casolari, Andrea Cuoghi and Adriana Munteanu for help in the laboratory. We thank Simona Bigi and Simona Marchetti-Dori for formal analyses. We also thank Europomice srl, Milano (Italy), especially Dr. Carlo Maffei and Dr. Bruno Maggi for materials supply and financial support for one year of doctoral scholarship of Fabiana Altimari (CUPE85F21003350001).

Data availability

Data will be made available on request.

References

[1] UN, THE 17 GOALS | sustainable development. https://sdgs.un.org/goals, 2024, 7.23.24.
[2] M. Tayebi-Khorami, M. Edraki, G. Corder, A. Golev, Re-thinking mining waste through an integrative approach led by circular economy aspirations, Minerals 9 (2019) 286, https://doi.org/10.3390/min9050286.
[3] F. Altimari, F. Andreola, P.P. Benassi, I. Lancellotti, L. Barbieri, Pumice and lapillus scraps: new national environmental-friendly chance for the production of ceramic tiles, Ceram. Int. 49 (2023) 38743–38753, https://doi.org/10.1016/j.ceramint.2023.09.211.
[4] G. Galamini, D. Malferrari, F. Altimari, S. Orlandi, L. Barbieri, From quarry by-products to a zeolites-based Zn fertilizer with increased resistance to rain leaching, Microporous Mesoporous Mater. 379 (2024) 113290, https://doi.org/10.1016/j.micromeso.2024.113290.
[5] G. Galamini, G. Ferretti, V. Medoro, N. Eftekhari, M. Favero, B. Faccini, M. Coltorti, Applying natural and K-enriched zeolite before struvite precipitation improved the recovery of NH_4^+ from liquid digestate and the reagent use efficiency, Int. J. Environ. Res. 18 (2024) 44, https://doi.org/10.1007/s41742-024-00595-5.
[6] A.M. Rashad, A short manual on natural pumice as a lightweight aggregate, J. Build. Eng. 25 (2019) 100802, https://doi.org/10.1016/j.jobe.2019.100802.
[7] Ö. Salli Bideci, A. Bideci, A.H. Gültekin, S. Oymael, H. Yildirim, Polymer coated pumice aggregates and their properties, Compos. B Eng. 67 (2014) 239–243, https://doi.org/10.1016/j.compositesb.2013.10.009.
[8] L. Barbieri, F. Altimari, F. Andreola, B. Maggi, I. Lancellotti, Characterization of volcano-sedimentary rocks and related scraps for design of sustainable materials, Materials 16 (2023) 3408, https://doi.org/10.3390/ma16093408.
[9] Directive 2008/98/EC, OJL, 2008.
[10] DL 152/2006. https://www.normattiva.it/uri-res/N2Ls?urn:nir:stato:decreto.legislativo:2006-04-03;152, 2006, 12.21.23.
[11] DPR 120/2017. https://www.normattiva.it/uri-res/N2Ls?urn:nir:stato:decreto.del.presidente.della.repubblica:2017-06-13;120!vig=, 2017, 12.21.23.
[12] F.N. Değirmenci, A. Yılmaz, Use of Pumice Fine Aggregate as an Alternative to Standard Sand in Production of Lightweight Cement Mortar, 2011.
[13] A.M. Rashad, An overview of pumice stone as a cementitious material – the Best Manual for Civil Engineer, Silicon 13 (2021) 551–572, https://doi.org/10.1007/s12633-020-00469-3.
[14] H.K. Alzaidy, F.M. Al Khatib, A.S. Dawood, The use of a pumice stone in removal of petroleum hydrocarbons from industrial wastewater through coagulation and flocculation, Environ Health Eng Manag 10 (2023) 141–147, https://doi.org/10.34172/EHEM.2023.16.
[15] D.A. LindaNtangu, I.J. Macha, Potential use of pumice rocks for municipal and industrial wastewater treatment in Tanzania, Int. J. Environ. Sci. Technol. 20 (2023) 2551–2562, https://doi.org/10.1007/s13762-022-04148-1.
[16] E. Galli, E. Passaglia, Natural zeolites in environmental engineering, in: H. Holzapfel (Ed.), Zeolites in Chemical Engineering. Process Eng Engineering GmbH, 2011, pp. 392–416.
[17] G. Gottardi, E. Galli, Natural Zeolites, Minerals and Rocks, Springer-Verlag, Berlin Heidelberg NewYork Tokio, 1985.
[18] T. Derbe, S. Temesgen, M. Bitew, A short review on synthesis, characterization, and applications of zeolites, Adv. Mater. Sci. Eng. 2021 (2021) 6637898, https://doi.org/10.1155/2021/6637898.
[19] V. Inglezakis, A. Zorpas (Eds.), Handbook of Natural Zeolites, Bentham Science Publishers, 2012, https://doi.org/10.2174/9781608052615112010101.
[20] A. Mahler, Zeolites: Advances in Research and Applications, Geology and Mineralogy Research Developments, Nova Science Publishers, New York, 2020.
[21] F.A. Mumpton, Mineralogy and geology of natural zeolites, Rev. Mineral. Geochem. 4 (2019) 1–201.
[22] R.T. Pabalan, F.P. Bertetti, Cation-exchange properties of natural zeolites, Rev. Mineral. Geochem. 45 (2001) 453–518, https://doi.org/10.2138/rmg.2001.45.14.
[23] Natural zeolites: occurrence, properties, applications, in: D.L. Bish, D.W. Ming (Eds.), Reviews in Mineralogy and Geochemistry, Mineralogical Society of America, Washington, DC, 2001.
[24] D. Malferrari, A. Laurora, M.F. Brigatti, M. Coltorti, D. Di Giuseppe, B. Faccini, E. Passaglia, M.G. Vezzalini, Open-field experimentation of an innovative and integrated zeolitite cycle: project definition and material characterization, Rendiconti Lincei 24 (2013) 141–150, https://doi.org/10.1007/s12210-013-0235-3.
[25] H.M.A. El-Lateef, M. Gouda, M.M. Khalaf, S. Shaaban, N.A.A. Elkanzi, E.S.A. Saber, A.A. Abdelhamid, A.M. Ali, Pumice as a novel natural heterogeneous catalyst for the designation of 3,4-dihydropyrimidine-2-(1H)-ones/thiones under solvent-free conditions, Molecules 27 (2022) 6044, https://doi.org/10.3390/molecules27186044.
[26] Q. Ke, F. Xiong, G. Fang, J. Chen, X. Niu, P. Pan, G. Cui, H. Xing, H. Lu, The reinforced separation of intractable gas mixtures by using porous adsorbents, Adv. Mater. (2024) 2408416, https://doi.org/10.1002/adma.202408416.
[27] R. Kumar, A. Srivastava, R. Lakhani, Industrial wastes-cum-strength enhancing additives incorporated lightweight aggregate concrete (LWAC) for energy efficient building: a comprehensive review, Sustainability 14 (2021) 331, https://doi.org/10.3390/su14010331.
[28] R. Wei, T. Alshahrani, B. Chen, A.B. Ibragimov, H. Xu, J. Gao, Advances in porous materials for efficient separation and purification of flue gas, Separ. Purif. Technol. 352 (2025) 128238, https://doi.org/10.1016/j.seppur.2024.128238.
[29] D.T. Zewdie, Y.D. Bizualem, A.G. Nurie, A review on removal CO2, SO2, and H2S from flue gases using zeolite based adsorbents, Discov. Appl. Sci. 6 (2024) 331, https://doi.org/10.1007/s42452-024-05989-w.
[30] S. Zhang, L. Yao, B. Xu, L. Yang, Z. Dai, W. Jiang, Recent advances in zeolite-based materials for volatile organic compounds adsorption, Separ. Purif. Technol. 350 (2024) 127742, https://doi.org/10.1016/j.seppur.2024.127742.
[31] E. Cataldo, L. Salvi, F. Paoli, M. Fucile, G. Masciandaro, D. Manzi, C.M. Masini, G. B. Mattii, Application of zeolites in agriculture and other potential uses: a review, Agronomy 11 (2021), https://doi.org/10.3390/agronomy11081547.
[32] N. Eroglu, M. Emekci, C.G. Athanassiou, Applications of natural zeolites on agriculture and food production, J. Sci. Food Agric. 97 (2017) 3487–3499, https://doi.org/10.1002/jsfa.8312.
[33] G. Galamini, G. Ferretti, C. Rosinger, S. Huber, V. Medoro, A. Mentler, E. Díaz-Pinés, M. Gorfer, B. Faccini, K.M. Keiblinger, Recycling nitrogen from liquid digestate via novel reactive struvite and zeolite minerals to mitigate agricultural pollution, Chemosphere 317 (2023) 137881, https://doi.org/10.1016/J.CHEMOSPHERE.2023.137881.
[34] Z. Ghasemi, I. Sourinejad, H. Kazemian, S. Rohani, Application of zeolites in aquaculture industry: a review, Rev. Aquacult. 10 (2018) 75–95, https://doi.org/10.1111/raq.12148.
[35] S. Hazrati, Z. Tahmasebi-Sarvestani, A. Mokhtassi-Bidgoli, S.A.M. Modarres-Sanavy, H. Mohammadi, S. Nicola, Effects of zeolite and water stress on growth, yield and chemical compositions of *Aloe vera* L, Agric. Water Manag. 181 (2017) 66–72, https://doi.org/10.1016/j.agwat.2016.11.026.
[36] R. Jarosz, J. Szerement, K. Gondek, M. Mierzwa-Hersztek, The use of zeolites as an addition to fertilisers – a review, Catena (Cremling.) 213 (2022), https://doi.org/10.1016/j.catena.2022.106125.
[37] A. Lateef, R. Nazir, N. Jamil, S. Alam, R. Shah, M.N. Khan, M. Saleem, Synthesis and characterization of zeolite based nano–composite: an environment friendly slow release fertilizer, Microporous Mesoporous Mater. 232 (2016) 174–183, https://doi.org/10.1016/j.micromeso.2016.06.020.
[38] D. Malferrari, A. Laurora, M.F. Brigatti, D. Di Giuseppe, B. Faccini, M. Coltorti, A time- and cost-saving method to check the point-to-point distribution of soil improvers, J. Plant Nutr. Soil Sci. (2021), https://doi.org/10.1002/jpln.202000409.
[39] G. Galamini, G. Ferretti, C. Rosinger, S. Huber, A. Mentler, E. Diaz–Pines, B. Faccini, K.M. Keiblinger, Potential for agricultural recycling of struvite and zeolites to improve soil microbial physiology and mitigate CO2 emissions, Geoderma (Amst.) 453 (2025) 117149, https://doi.org/10.1016/j.geoderma.2024.117149.
[40] T. Campisi, F. Abbondanzi, B. Faccini, D. Di Giuseppe, D. Malferrari, M. Coltorti, A. Laurora, E. Passaglia, Ammonium-charged zeolitite effects on crop growth and nutrient leaching: greenhouse experiments on maize (Zea mays), Catena (Cremling.) 140 (2016) 66–76, https://doi.org/10.1016/j.catena.2016.01.019.
[41] B. Faccini, D. Di Giuseppe, D. Malferrari, M. Coltorti, F. Abbondanzi, T. Campisi, A. Laurora, E. Passaglia, Ammonium-exchanged zeolitite preparation for agricultural uses: from laboratory tests to large-scale application in ZeoLIFE project prototype, Period. Mineral. 84 (2015) 303–321, https://doi.org/10.2451/2015PM0015.
[42] G. Ferretti, M. Alberghini, G. Galamini, V. Medoro, B. Faccini, S. Balzan, M. Coltorti, Exploring the combined effects of different nitrogen sources and chabazite zeolite-tuff on nitrogen dynamics in an acidic sandy-loam soil, Soil Syst. 8 (2024) 16, https://doi.org/10.3390/soilsystems8010016.
[43] G. Ferretti, G. Galamini, V. Medoro, B. Faccini, Amount and speciation of N leached from a sandy soil fertilized with urea, liquid digestate, struvite and NH_4-enriched chabazite zeolite-tuff, Soil Use Manag. 39 (2023) 456–473, https://doi.org/10.1111/sum.12855.
[44] V. Medoro, G. Ferretti, G. Galamini, A. Rotondi, L. Morrone, B. Faccini, M. Coltorti, Reducing nitrogen fertilization in olive growing by the use of natural chabazite-zeolitite as soil improver, Land 11 (2022) 1471, https://doi.org/10.3390/land11091471.
[45] F. Calzarano, L. Seghetti, G. Pagnani, S. Di Marco, Italian zeolitites in the control of grey mould and sour rot and their effect on leaf reflectance, grape and wine, Agriculture 10 (2020) 580, https://doi.org/10.3390/AGRICULTURE10120580, 2020 10, 580.
[46] F. Calzarano, G. Valentini, G. Arfelli, L. Seghetti, A.C. Manetta, E.G. Metruccio, S. Di Marco, Activity of Italian natural chabasite-rich zeolitites against grey mould, sour rot and grapevine moth, and effects on grape and wine composition, Phytopathol. Mediterr. 58 (2019) 309–323, https://doi.org/10.14601/Phytopathol_Mediter-10618.

[47] E. Cataldo, M. Fucile, G.B. Mattii, Leaf eco-physiological profile and berries technological traits on potted vitis vinifera L. cv Pinot Noir Subordinated to Zeolite Treatments under Drought Stress, Plants 11 (2022) 1735, https://doi.org/10.3390/plants11131735.
[48] C. De Smedt, E. Someus, P. Spanoghe, Potential and actual uses of zeolites in crop protection, Pest Manag. Sci. 71 (2015) 1355–1367, https://doi.org/10.1002/ps.3999.
[49] D.M. Glenn, G. Puterka, Particle film technology: an overview of history, concepts and impact in horticulture, Acta Hortic. 636 (2004) 509–511, https://doi.org/10.17660/ActaHortic.2004.636.63.
[50] D.G. Petoumenou, Enhancing yield and physiological performance by foliar applications of chemically inert mineral particles in a rainfed vineyard under mediterranean conditions, Plants 12 (2023) 1444, https://doi.org/10.3390/plants12071444.
[51] A. Rotondi, G. Bertazza, B. Faccini, G. Ferretti, L. Morrone, Effect of different foliar particle films (kaolin and zeolitite) on chemical and sensory properties of olive oil, Agronomy 12 (2022) 3088, https://doi.org/10.3390/agronomy12123088.
[52] N. Shahsavari, A. Dadrasnia, Effect of zeolites and zinc on the physiological characteristics of canola under late-season drought stress, Commun. Soil Sci. Plant Anal. 47 (2016) 2077–2087, https://doi.org/10.1080/00103624.2016.1228940.
[53] L. Morrone, L. Neri, O. Facini, G. Galamini, G. Ferretti, A. Rotondi, Influence of chabazite zeolite foliar applications on olive fly control, volatile organic compounds emission and quality of extra virgin olive oil, Plants 13 (5) (2024) 698, https://doi.org/10.3390/plants13050698.
[54] P. Subedi, E.J. Jokela, J.G. Vogel, R. Bracho, K.S. Inglett, The effects of nutrient limitations on microbial respiration and organic matter decomposition in a Florida Spodosol as influenced by historical forest management practices, For. Ecol. Manag. 479 (2021) 118592, https://doi.org/10.1016/j.foreco.2020.118592.
[55] A. Neupane, E.M. Herndon, T. Whitman, A.M. Faiia, S. Jagadamma, Manganese effects on plant residue decomposition and carbon distribution in soil fractions depend on soil nitrogen availability, Soil Biol. Biochem. 178 (2023) 108964, https://doi.org/10.1016/j.soilbio.2023.108964.
[56] Y. Zong, Z. Li, R. Gui, D. Chen, M. Yuan, Y. Chai, S. Shan, M.H. Wong, Manganese losses induced by severe soil acidification in the extensive Lei bamboo (Phyllostachys violascens) plantation stands in Eastern China, Chemosphere 339 (2023) 139669, https://doi.org/10.1016/j.chemosphere.2023.139669.
[57] Zhen Zhang, Zhongming Zhang, H. Chen, J. Liu, C. Liu, H. Ni, C. Zhao, M. Ali, F. Liu, L. Li, Surface Mn(II) oxidation actuated by a multicopper oxidase in a soil bacterium leads to the formation of manganese oxide minerals, Sci. Rep. 5 (2015) 10895, https://doi.org/10.1038/srep10895.
[58] S. Alejandro, S. Höller, B. Meier, E. Peiter, Manganese in plants: from acquisition to subcellular allocation, Front. Plant Sci. 11 (2020), https://doi.org/10.3389/fpls.2020.00300.
[59] E.F. Santos, J.M. Kondo Santini, A.P. Paixão, E.F. Júnior, J. Lavres, M. Campos, A. R.D. Reis, Physiological highlights of manganese toxicity symptoms in soybean plants: Mn toxicity responses, Plant Physiol. Biochem. 113 (2017) 6–19, https://doi.org/10.1016/j.plaphy.2017.01.022.
[60] S. López-Rayo, P. Nadal, J.J. Lucena, Novel chelating agents for iron, manganese, zinc, and copper mixed fertilisation in high pH soil-less cultures, J. Sci. Food Agric. 96 (2016) 1111–1120, https://doi.org/10.1002/jsfa.7183.
[61] V. Brusko, B. Garifullin, G. Geniyatullina, P. Kuryntseva, G. Galieva, P. Galitskaya, S. Selivanovskaya, A.M. Dimiev, Novel biodegradable chelating agents for micronutrient fertilization, J. Agric. Food Chem. 71 (2023) 14979–14988, https://doi.org/10.1021/acs.jafc.3c03500.
[62] S. López-Rayo, S. Lucena, J.J. Lucena, Chemical properties and reactivity of manganese chelates and complexes in solution and soils, J. Plant Nutr. Soil Sci. 177 (2014) 189–198, https://doi.org/10.1002/jpln.201300091.
[63] M.H. Rashed, T. Hoque, M.M.R. Jahangir, M. Hashem, Manganese as a micronutrient in agriculture: crop requirement and management, Journal of Environmental Science and Natural Resources 12 (2021) 225–242, https://doi.org/10.3329/jesnr.v12i1-2.52040.
[64] A.F. Gualtieri, G.D. Gatta, R. Arletti, G. Artioli, P. Ballirano, G. Cruciani, A. Guagliardi, D. Malferrari, N. Masciocchi, P. Scardi, Quantitative phase analysis using the Rietveld method: towards a procedure for checking the reliability and quality of the results, Period. Mineral. 88 (2019), https://doi.org/10.2451/2019PM870.
[65] H.D. Young, Statistical Treatment of Experimental Data, McGraw-Hill Book Company, New York, 1962.
[66] N. Kloster, M. Perez, F. Mazzaferro, A rapid and simple manifold to study exchangeable cations and cation exchange capacity in 24 soil samples simultaneously, Commun. Soil Sci. Plant Anal. 50 (2019) 1500–1511, https://doi.org/10.1080/00103624.2019.1631329.
[67] ISO/DIS 22171, n.d. Soil Quality — Determination of Potential Cation Exchange Capacity (CEC) and Exchangeable Cations Buffered at pH 7, Using a Molar Ammonium Acetate Solution.
[68] J.D. Hem, Chemical factors that influence the availability of iron and manganese in aqueous systems, GSA Bulletin 83 (1972) 443–450, https://doi.org/10.1130/0016-7606(1972)83[443:CFTITA]2.0.CO;2.
[69] A. Conti, E. Sacchi, M. Chiarle, G. Martinelli, G.M. Zuppi, Geochemistry of the formation waters in the Po plain (northern Italy): an overview, Appl. Geochem. 15 (2000) 51–65, https://doi.org/10.1016/S0883-2927(99)00016-5.
[70] M.M. Malhado Simões Ribeiro, The cenozoic aquifer system of the Lower Tagus Basin: a description of the hydrogeological situation in the Almada region (Portugal), Hydrogeol. J. 17 (2009) 999–1009, https://doi.org/10.1007/s10040-009-0450-2.
[71] R Core Team, R: A Language and Environment for Statistical Computing, R Foundation for Statistical Computing, Vienna, Austria, 2021. https://www.R-project.org/.
[72] J.R.V. Saroyda, R.Y.S. Cruz, R.J.C. Antonio, C.L.P. Flestado, J.R.S. Magalong, K.Z. P. Zagala, C.L. Barbacena, J.M. Bumatay, L.F. Bautista, C.C. Deocaris, Pupaim. https://CRAN.R-project.org/package=PUPAIM, 2001.
[73] J.R. Magalong, J. DelaCruz, J. Bumatay, C. Deocaris, PUPAK: Parameter Estimation, and Plot Visualization of Adsorption Kinetic Models, 2022, https://doi.org/10.32614/CRAN.package.PUPAK.
[74] G. Gottardi, E. Galli, Natural zeolites, Geological Magazine, Minerals and Rocks Series 18 (2009) 718, https://doi.org/10.1017/S0016756800024456.
[75] F. Yang, R. Coates, G.C. Boles, P.B. Armentrout, Thermochemical studies of hydrated manganese dications, Mn2+(H2O)x (x = 4–9), using guided ion beam tandem mass spectrometry, Int. J. Mass Spectrom. 468 (2021) 116638, https://doi.org/10.1016/j.ijms.2021.116638.
[76] R.P. Townsend, E.N. Coker, Chapter 11 Ion exchange in zeolites, in: H. van Bekkum, E.M. Flanigen, P.A. Jacobs, J.C. Jansen (Eds.), Studies in Surface Science and Catalysis, Introduction to Zeolite Science and Practice, Elsevier, 2001, pp. 467–524, https://doi.org/10.1016/S0167-2991(01)80253-6.
[77] N. Kantiranis, A. Filippidis, S. Vouta, A. Drakoulis, T. Koutles, E. Tzamos, The cation exchange capacity of industrial minerals and rocks of Milos Island, Bull. Geol. Soc. Greece 40 (2007) 775–780, https://doi.org/10.12681/bgsg.16718.
[78] J. Sterba, G. Steinhauser, M. Bichler, Cation-exchange properties of pumice - taking a sip from a volcanic cocktail, J. Radioanal. Nucl. Chem. 276 (2008) 175–178, https://doi.org/10.1007/s10967-007-0428-2.
[79] G. Asgari, B. Roshani, G. Ghanizadeh, The investigation of kinetic and isotherm of fluoride adsorption onto functionalize pumice stone, J. Hazard Mater. 217–218 (2012) 123–132, https://doi.org/10.1016/j.jhazmat.2012.03.003.
[80] G. Mucsi, A review on mechanical activation and mechanical alloying in stirred media mill, Chem. Eng. Res. Des. 148 (2019) 460–474, https://doi.org/10.1016/j.cherd.2019.06.029.
[81] R. Szabó, F. Kristály, S. Nagy, R. Singla, G. Mucsi, S. Kumar, Reaction, structure and properties of eco-friendly geopolymer cement derived from mechanically activated pumice, Ceram. Int. 49 (2023) 6756–6763, https://doi.org/10.1016/j.ceramint.2022.10.204.
[82] J.P. Vareda, On validity, physical meaning, mechanism insights and regression of adsorption kinetic models, J. Mol. Liq. 376 (2023) 121416, https://doi.org/10.1016/j.molliq.2023.121416.
[83] J.P. Simonin, On the comparison of pseudo-first order and pseudo-second order rate laws in the modeling of adsorption kinetics, Chem. Eng. J. Amsterdam, Neth 300 (2016) 254–263, https://doi.org/10.1016/j.cej.2016.04.079.
[84] H.N. Tran, S.-J. You, A. Hosseini-Bandegharaei, H.-P. Chao, Mistakes and inconsistencies regarding adsorption of contaminants from aqueous solutions: a critical review, Water Res. 120 (2017) 88–116, https://doi.org/10.1016/j.watres.2017.04.014.
[85] L. Largitte, R. Pasquier, A review of the kinetics adsorption models and their application to the adsorption of lead by an activated carbon, Chem. Eng. Res. Des. 109 (2016) 495–504, https://doi.org/10.1016/j.cherd.2016.02.006.
[86] H.I. Inyang, A. Onwawoma, S. Bae, The Elovich equation as a predictor of lead and cadmium sorption rates on contaminant barrier minerals, Soil Tillage Res. 155 (2016) 124–132, https://doi.org/10.1016/j.still.2015.07.013.
[87] M. Noroozifar, M. Khorasani-Motlagh, H. Naderpour, Modified nanocrystalline natural zeolite for adsorption of arsenate from wastewater: isotherm and kinetic studies, Microporous Mesoporous Mater. 197 (2014) 101–108, https://doi.org/10.1016/j.micromeso.2014.05.037.
[88] Z. Alothman, A review: fundamental aspects of silicate mesoporous materials, Materials 5 (2012) 2874–2902, https://doi.org/10.3390/ma5122874.
[89] M. Hadi, G. Mckay, M.R. Samarghandi, A. Maleki, M. Aminabad, Prediction of optimum adsorption isotherm: comparison of chi-square and Log-likelihood statistics, Desalination Water Treat. 49 (2012) 81–94, https://doi.org/10.1080/19443994.2012.708202.
[90] R. Saadi, Z. Saadi, R. Fazaeli, N. Elmi Fard, Monolayer and multilayer adsorption isotherm models for sorption from aqueous media, Kor. J. Chem. Eng. 32 (2015), https://doi.org/10.1007/s11814-015-0053-7.
[91] N. Mansouri, N. Rikhtegar, H. Panahi, F. Atabi, B. Karimi Shahraki, Porosity, characterization and structural properties of natural zeolite - clinoptilolite - as a sorbent, Environ. Protect. Eng. 39 (2013) 139, https://doi.org/10.5277/EPE130111.
[92] F.-C. Wu, R.-L. Tseng, R.-S. Juang, Initial behavior of intraparticle diffusion model used in the description of adsorption kinetics, Chem. Eng. J. (Amsterdam, Neth.) 153 (2009) 1–8, https://doi.org/10.1016/j.cej.2009.04.042.
[93] D. Malferrari, S. Poppi, Product for Defending and Feeding Plants and Respective Preparation Method and Use, 2017. EP3238541 (A1).